Measuring Turbulent Dissipation Using a Tethered ADCP

Lucas, N.S.; Simpson, J.H.; Rippeth, T.P.

Journal of Atmospheric and Oceanic Technology

Cyswllt i'r cyhoeddiad / Link to publication

Measuring Turbulent Dissipation Using a Tethered ADCP

N. S. LUCAS, J. H. SIMPSON, AND T. P. RIPPETH

Bangor University, School of Ocean Sciences, Anglesey, United Kingdom

C. P. OLD

University of Edinburgh, Edinburgh, United Kingdom

ABSTRACT

The structure function method for estimating the dissipation rate of turbulent kinetic energy, previously validated for measurements from seabed fixed mounts, is applied to data from 1.2-MHz acoustic Doppler current profiler (ADCP) instruments operating in pulse–pulse coherent mode and mounted in midwater below a tethered buoy. Movements of the buoy introduce additional relative velocity components, but it is hypothesized that these flow components should not seriously interfere with the turbulence information because (i) horizontal or vertical translation induces the same flow component in all cells of an ADCP beam and (ii) any rotation of the instrument about its center induces flow components that are normal to the beam direction, and thus neither affect the structure function. This hypothesis is tested by comparing a series of dissipation measurements from a moored ADCP with those from a free-falling Vertical Microstructure Profiler (VMP) shear probe deployed from a nearby research vessel. The results indicate generally good conformity in both mean and variability over almost two decades of dissipation rates. The noise level of the structure function estimates with the pulse–pulse coherent ADCP is close to that of the VMP at $\sim 3 \times 10^{-10}\,\mathrm{W\,kg^{-1}}$. This approach offers the prospect of long time series measurements of dissipation rate from moorings, albeit with restricted vertical range of a few meters.

1. Introduction

Vertical exchange driven by turbulent mixing is a key process in determining momentum and heat fluxes and material transport pathways in the marine environment. In recent years, our ability to measure a turbulence parameter, the rate of dissipation of turbulent kinetic energy, has led to major advances in our understanding of the vertical exchange processes and their parameterization (Burchard et al. 1998; MacKinnon and Gregg 2003; Sharples et al. 2001; Simpson et al. 1996). These advances have largely been based on profile measurements made using free-falling microstructure profilers. The major drawback of such measurements is that they

are labor intensive and require a dedicated ship. Datasets thus tend to be sparse and intermittent and rarely exceed one or two days duration.

In recent years, acoustic Doppler current profilers (ADCPs) have been increasingly applied to the measurement of turbulent parameters. In the "variance method," the shear stress in the flow above a bottom-mounted ADCP is estimated from the difference of velocity variance in the opposing ADCP beams (Stacey et al. 1999; Lu et al. 2000; Rippeth et al. 2002; Howarth and Souza 2005; Williams and Simpson 2004) in a technique analogous to that used in stress measurements in radar meteorology. The rate of turbulent energy production is obtained from the product of the shear stress and the vertical shear of velocity, which is also measured by the ADCP. A restriction in the application of the variance method is that the analysis requires that the ADCP be mounted on the seabed or a rigid platform and carefully levelled with the axis of instrument aligned to $\sim 1^\circ$ of the vertical, a requirement that can usually be met by the use of a gimbal mounting in the ADCP frame.

In the structure function (SF) method (Wiles et al. 2006), differences in the along-beam velocities between bins are used to derive an estimate of ε, the rate of TKE dissipation. The analysis requires that the differences are taken over bin separations that lie within the inertial subrange of the turbulence spectrum (i.e., the range of scales within which the turbulence can be considered isotropic). This concentration on motions that are isotropic means that there is no requirement for a particular orientation, which is an important advantage over the variance method. The range of scales in the inertial subrange is set at the lower end by the Kolmogorov microscale L_K, which is usually <1 cm, and at the upper end in stratified turbulence by the Ozmidov length $L_o = \sqrt{\varepsilon/N^3}$, which depends on water column stratification through the stability frequency N. It is worth noting that this restricted focus on isotropic motions in the inertial subrange applies equally in the interpretation of shear probe measurements (Baumert et al. 2005) and the fitting of turbulent energy spectra to the Kolmogorov $k^{-5/3}$ form.

The structure function method has been validated by comparisons between measurements made from bed-mounted ADCP and shear probe profile instruments in energetic tidal flows with weak stratification (Wiles et al. 2006). Mohrholz et al. (2008) have applied the SF method to data from a pulse-coherent Doppler (pc-ADP) observations of near-bed flows in descending plumes in the Baltic. Their results provide convincing evidence of close agreement between dissipation measured (i) by the structure function, (ii) by fitting of the inertial subrange spectra from acoustic Doppler velocimetry (ADV) measurements, and (iii) from shear profiles with a mean square slope (MSS) microstructure probe. The use of the pulse-to-pulse coherent technique greatly reduces noise levels but restricts the working range to a few meters. Applying the SF method to coherent Doppler measurements allows, for example, the determination of the low dissipation rates driven by seiche motions in the bottom boundary of lakes (Lorke 2007; Lorke et al. 2008; Simpson et al. 2011).

This contribution looks at the possibility of taking the SF method one step further by using an ADCP in pulse coherent mode to measure dissipation in midwater. In this case, the instrument has to be mounted on a buoyant tether and will move around in the flow and so experience relative motions that could contaminate the structure function. After briefly reprising the basis of the SF analysis in section 2, we consider the effect of the relative motions of a tethered instrument (section 3) before describing the observational methods and the environment of the chosen site (4). The results are presented in section 5, which is followed by a concluding
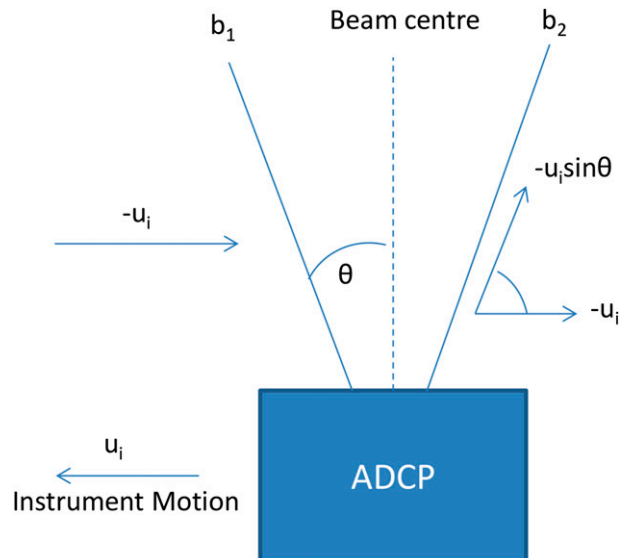

FIG. 1. ADCP relative velocities components induced by instrument motion u_i.

section that interprets the results and discusses their implications.

2. The structure function approach

ADCPs measure the water velocity along the direction of their acoustic beams by determining the Doppler shift of the returned signal from range-gated cells. Employing the single-pulse technique, ADCPs measure the Doppler frequency shift of back-scattered acoustic pings to estimate velocities of scattering particles. In the pulse–pulse coherent mode utilized here, the phase shift between two pings is correlated. This results in much improved range resolution and low standard deviations of velocity estimates but at the expense of profiling range, which is restricted by the classical range–velocity ambiguity relation $r_{max}V_{max} = \pm c\lambda/8$, where c is the speed of sound in the medium and λ is the sonar wavelength (Lhermitte and Serafin 1984).

In conventional operation, the along-beam velocity components are converted to Cartesian components in x, y, and z. In the structure function method (Wiles et al. 2006; Rippeth et al. 2003) the raw along-beam velocity components $v(z)$ from each beam are used to estimate a second-order structure defined as

$$D(z,r) = \overline{[v'(z) - v'(z+r)]^2}, \qquad (1)$$

where $v' = v(z) - \overline{v}(z)$ is the fluctuating component of velocity at position z along the beam. Note that $D(z,r)$ is the mean square of the velocity fluctuation difference between two points separated by a distance r. For
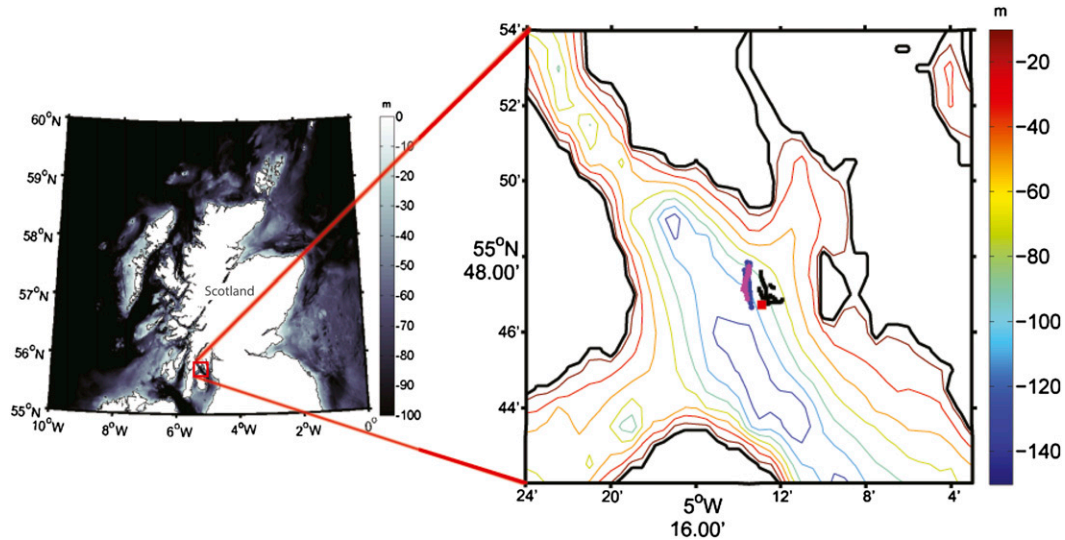
FIG. 2. Map and bathymetry of the observation area. Contours are shown in 20-m spacing from 10 to 130 m. Illustrated are the mooring position (red square) and VMP transects from each day, 14 (YD 257; black) 15 (YD 258; blue), and 16 September (YD 259; magenta).

isotropic turbulence, the structure function D is related to the dissipation ε by

$$D(z,r) = C_v^2 \varepsilon^{2/3} r^{2/3}, \tag{2}$$

where C_v is a constant. For a given ε, D should increase as $r^{2/3}$ from $D = 0$ at $r = 0$. In practice, $D \rightarrow M$ as $r \rightarrow 0$, where $M = 2\sigma_v^2$ is twice the variance of velocity estimates at a point due to instrumental noise of the ADCP. The observed $D(z, r)$ is therefore fitted to an equation of the form

$$D(z,r) = M + Ar^{2/3} \tag{3}$$

to estimate M and the dissipation ε from A according to

$$\varepsilon = \frac{A^{3/2}}{C_v^3}. \tag{4}$$

The constant C_v is taken to have a value of 1.45, which was determined from Doppler radar measurements of turbulence in the atmosphere (Sauvageot 1992). Confirmation of the applicability of this value in the ocean is given in Rippeth et al. (2003).

Dissipation values derived from the structure function from four beams, which may differ according to orientation relative to shear stress in the flow (Wiles et al. 2006), are usually averaged to provide a best estimate of ε at each depth level. An alternative is to combine the fluctuating velocity data from all four beams in a composite random variable b':

$$b' = (v_1' + v_2' - v_3' - v_4')/2, \tag{5}$$

where v_1' and v_2', and v_3' and v_4', are the fluctuating velocity components in opposing beam pairs. Using Eq. (5) and substituting b' into Eq. (1) we have for the structure function based on b':

$$D_e = \frac{1}{4}\overline{[v_1'(z) - v_1'(z+r) + v_2'(z) - v_2'(z+r) - v_3'(z) + v_3'(z+r) - v_4'(z) + v_4'(z+r)]^2}. \tag{6}$$

Now substitute $\Delta v_i' = v_i'(z) - v_i'(z+r)$ and expand:

$$D_e = \frac{1}{4}\{\overline{\Delta v_1'^2} + \overline{\Delta v_2'^2} + \overline{\Delta v_3'^2} + \overline{\Delta v_4'^2}\}$$
$$+ 2(\overline{\Delta v_1' \Delta v_2'} - \overline{\Delta v_1' \Delta v_3'} + \cdots). \tag{7}$$

On the assumption that the turbulent velocity fluctuations in the beams are independent and as such have zero covariance, the mean cross-product terms will be zero and hence the structure function D_e will be equivalent to the average SF of the four beams. The assumption of independence may be justified by the

separation of the ADCP beams, which ranges from 0.72 to 1.70 m in the measurement volume.

The variance of the fluctuations is maintained through dividing by a factor of $\sqrt{n} = \sqrt{4} = 2$. The variable b' is closely related to the "error velocity" (RD Instruments 1998; Gilcoto et al. 2009), which is defined as

$$e_{RDI} = \frac{1}{2\sqrt{2}\sin\theta}(v'_1 + v'_2 - v'_3 - v'_4) = \frac{b'}{\sqrt{2}\sin\theta}. \quad (8)$$

The error velocity is available when velocity data are recorded in Cartesian coordinates so that the structure function based on b' may be used to apply the method when the along-beam velocities have not been recorded.

3. Tethered ADCP operation

In contrast to ADCP measurements from fixed platforms or moorings located on the seabed, instruments tethered in midwater are free to move, thus inducing relative velocities that might be expected to compromise the determination to the structure function. We need to consider the effects of (i) translation of the ADCP "beam center" (see Fig. 1), both horizontally and vertically, and (ii) all forms of rotation of the instrument about the beam center. Underlying assumptions here are that the turbulence is spatially homogeneous on the scale of the beam separation and is statistically stationary over the sampling period.

For an instrument on a long tether, the principal motion will be horizontal displacements in x and y from an equilibrium position. If the instrument is moving through the water at a velocity u_i, the relative velocity seen by the ADCP will be $-u_i$, which will induce an along-beam component in beam 2 (Fig. 1). Each bin sees the same relative velocity, so this motion will be cancelled in the structure function, which is based on velocity differences. On shorter tethers, the oscillatory movement of a tethered instrument may also involve significant vertical displacements but here again all bins in a particular beam will see the same relative velocity so there should be no contribution to the structure function. The instrument will also rotate to some degree in the tethered motions, again inducing motions relative to the beams. The induced velocities for rotation about all three axes (pitch, roll, and yaw) are, however, all normal to the beams and so do not contribute observed along-beam velocities and so should not affect the structure function.

While the above arguments suggest that the motions of a tethered instrument should not seriously compromise the structure function approach to the determination of dissipation, there may be contamination of the data close to the instrument due to the local generation of turbulence
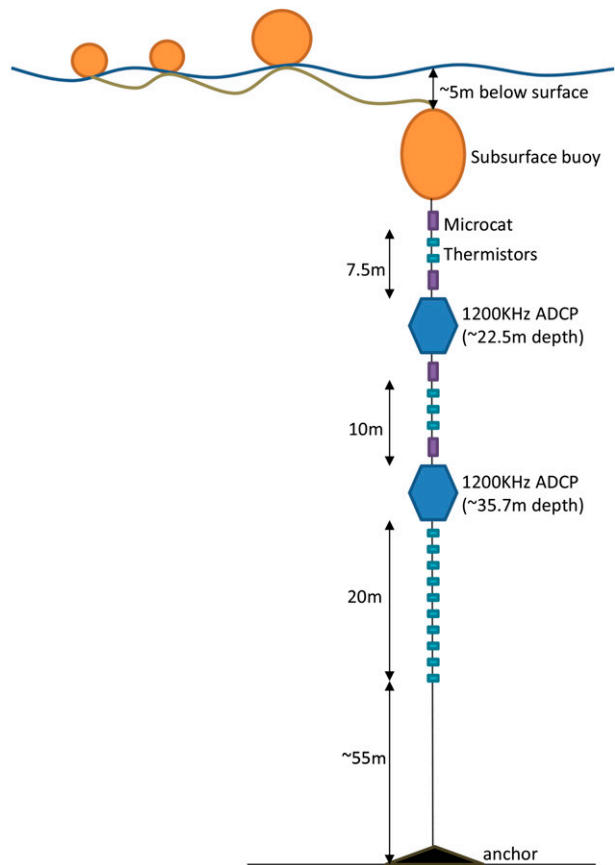

FIG. 3. Mooring configuration. Both ADCPs are mounted upward looking with Microcats positioned ~2 m above each. There were 15 temperature loggers at 2-m intervals and a further two Microcats centered at 2-m spacing.

in flow past the ADCP and its supporting buoy (Gartner and Ganju 2002). Reduced correlation and velocity bias near the transducer is well documented in acoustic research and is thought to be influenced by the complex field distribution in the near field, causing lateral beam modulation in amplitude and phase (Zedel et al. 1996; Lacy and Sherwood 2004; Li et al. 1997). Zedel et al. (1996) show that this can be attributed to the phase structure of the near-field beam introducing additional phase variance as targets are advected across the beam. This near-field zone boundary is expected for ranges less than $a^2 f/C$, where a is the transducer radius, f is the system frequency, and C is the speed of sound in water; thus, the near-field region should be blanked to remove this bias, which also effectively isolates the possibility of bias being incorporated into the analysis from turbulence created around the ADCP transducer.

4. Observations

The measurements reported here were made in the Clyde Sea, which is the largest of the Scottish fjords;
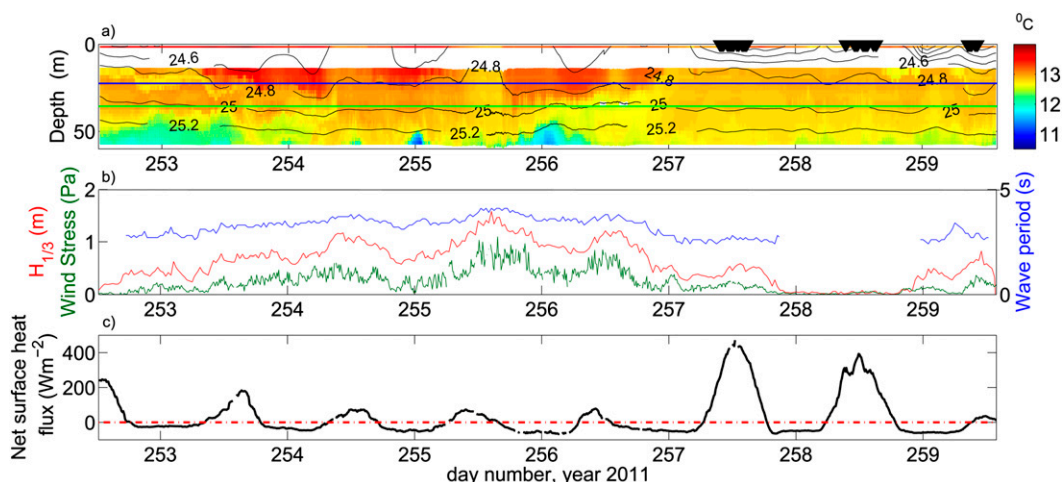
FIG. 4. The local conditions during the sampling period. (a) The color contoured thermal profile from 2-m spaced thermistors with overlaid interpolated isopycnals from Microcats centered at approximate depths of 15, 20.5, 24.1, and 33.7 m (black lines). The black triangles at the top of the plot represent the timings of the VMP casts. Approximate ADCP positions are shown (green and blue lines). (b) The wind stress (green), significant wave height (red), and wave period (blue, y axis on right-hand side). (c) The net surface heat flux calculated using Simpson and Bowers (1984).

a deep partially enclosed basin connected to the adjacent shelf sea across a shallow (45 m) entrance sill. The fjord undergoes thermal and haline stratification in the summer (Inall and Rippeth 2002) and low levels of dissipation. There is evidence of enhanced dissipation within the thermocline region (Inall and Rippeth 2002; Jackson and Elliott 2002) driven by an internal wave generated by the tidal flow over the entrance sill. Velocity data were collected by two tethered ADCP units on a single mooring at 55°47.13′N, 5°12.42′W, in a water depth of ~100 m (Fig. 2). The upper and lower ADCPs were mounted on in-line frames at mean depths of 22.5

and 35.7 m. The mooring (Fig. 3) was also instrumented with four Microcat sensors (measuring temperature and salinity) as well as temperature loggers at 2-m intervals.

The RD Instruments (RDI) Workhorse 1.2-MHz ADCPs were operated in high-resolution pulse–pulse coherent mode. Data were recorded in Earth coordinates using 5-cm depth bins, blanking distances of 44 cm, and ambiguity velocities of $0.05 \, \mathrm{m \, s^{-1}}$; the upper ADCP was sampling at a rate of 2 ping pairs per 1-s ensemble, while the lower ADCP was sampling at a rate of 3 ping pairs per 1.5-s ensemble. Two RDI algorithms were applied to the data during deployment: 1) a data
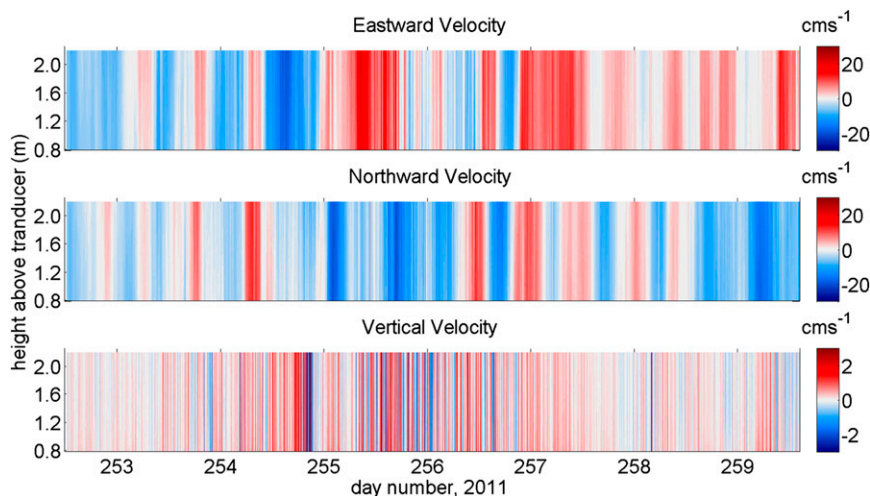

FIG. 5. The u, v, and w velocities for the upper ADCP (~22.5 m); note the different scale for the vertical velocities.
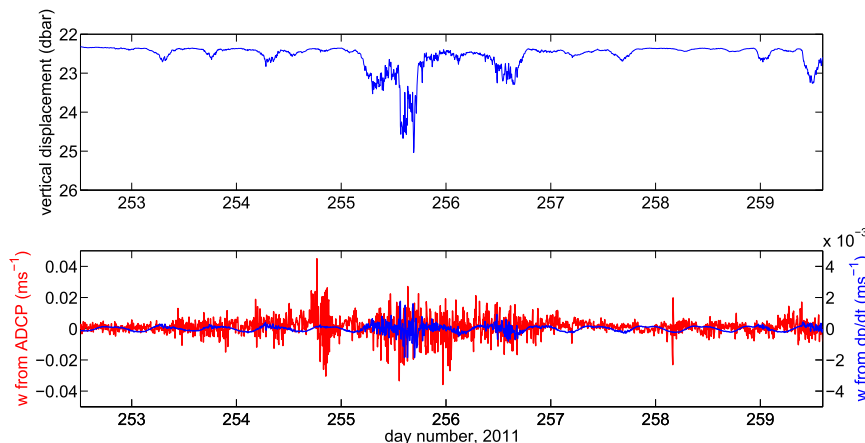
FIG. 6. Displacements for the upper ADCP. (top) The vertical excursion of the ADCP with the tidal signal removed. (bottom) The relative vertical velocities of the flow (red) and the mooring (blue), with data averaged over 5 min; note the different scales.

rejection analysis was applied to the raw ADCP data to exclude data that displayed a difference in echo intensity of >50 from the highest beam value, to account for losses due to fish interference in the beam path, and 2) RDI bin mapping was applied, which, when the instrument is tilted, uses the beam velocities from the bin nearest to the nominal (20°) bin center. Subsequent to this all data in the measurement volume that displayed a ping-to-ping correlation coefficient of below 0.7 were rejected, eliminating data collected with poor signal quality (Zedel et al. 1996). Finally, the structure function algorithm rejects data when there are less than three values for the $r^{2/3}$ fit.

Concurrent measurements of the turbulent dissipation through the water column were made with a Rockland Scientific Vertical Microstructure Profiler (VMP) shear probe. Dissipation was determined from the high-frequency velocity shear using standard processing techniques (Simpson et al. 1996) based on the relation

$$\varepsilon = 7.5\nu\overline{\left(\frac{\partial u}{\partial z}\right)^2}, \tag{9}$$

where ν is the kinematic viscosity of seawater.

There were a total of 98 VMP casts spread over 3 days indicated in Fig. 2. Casts were made with the vessel moving slowly ahead at ~0.25 m s^{-1} and staying close to the mooring; most profiles were taken within 1 km of the mooring with a maximum separation of ~2 km (see Fig. 2b).

5. Results

a. Surface forcing and density field

The mooring observations extended over a period of 7 days [year days (YD) 252–259] during which there were large changes in surface forcing (Fig. 4) due to the passage through the region of a low pressure system (the remains of Hurricane Katia) from the early hours of 12 September (YD 255) through to the evening of 13 September (YD 256). During this period, wind stress (Fig. 4b) increased to peak values of ~1 Pa with corresponding increases in wave height. Because of small fetch (~10 km or less), the development of the local sea was limited to relatively short waves with the dominant period increasing to 4.1 s during the storm (Fig. 2b). Net surface heat flux (Fig. 4c) was minimal during the storm period when solar radiation was reduced. In the calm period (from YD 257) following the storm, heat flux into the ocean increased considerably. This heat input together with a horizontal inflow of fresher water is reflected in the density contours (Fig. 4a), which show renewed stratification in the surface layers from YD 257 after the strong wind mixing during the storm.

b. Mean flow field

Contoured velocity data in Earth coordinates from the upper ADCP (Fig. 5) indicate the presence of semidiurnal tidal flows with amplitudes of ~7 cm s^{-1} prior to the storm period. During the storm, wind forced motions with peaks in horizontal current speed of up to ~30 cm s^{-1} predominated and regular semidiurnal reversal of the flow was not apparent. This situation continued for several days after the storm.

The upper limit of tilt during the worst of the storm reached 4.5° and 8.4° for the upper and lower ADCP respectively, which equates to a bin mapped translation at the extremities of the sampled range of two and three bins. However, the median tilts were 0.74° and 0.08° for the upper and lower ADCP, respectively; these values are below the threshold to trigger the RDI bin mapping
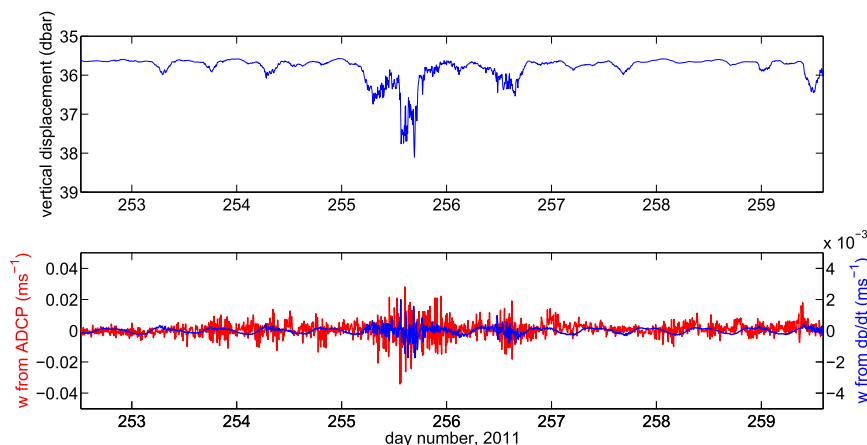
FIG. 7. As in Fig. 6, but for the lower ADCP.

algorithm. The vertical excursions of the ADCPs, plotted in the upper panels of Figs. 6 and 7, were estimated by removing the tidal signal from the pressure readings. The ADCP pressure signal was differentiated to obtain dp/dt and hence the vertical velocity of the mooring. This parameter, averaged over 300 s, is plotted in the lower panels of Figs. 6 and 7 in parallel with the averaged ADCP vertical velocity. It is clear that the water motions past the buoy greatly exceed the vertical movements of the buoy (note the different scales for w and dp/dt).

The vertical velocity w (Fig. 5c) exhibits substantial high-frequency motions with peak velocities of $\sim$4 cm s^{-1}. These motions of the water relative to the ADCP are seen to increase considerably during the storm period (Fig. 6). A spectral analysis of the vertical velocities for the whole time series from the upper ADCP, plotted in equal variance form in Fig. 8a, shows that the dominant contribution to w and dp/dt is in the surface

wave band with a broad spectral peak corresponding to the observed dominant wave period of $\sim$4 s. An alternative plot of the power spectral density versus $\log(f)$, Fig. 8b indicates a second weaker peak in w centered around 6×10^{-2} cycles min^{-1}. There is no corresponding response in the vertical movement of the mooring in this frequency band so this part of the w spectrum represents only internal water motions relative to a fixed reference.

c. Structure function and dissipation

The error velocities, from which b' and hence the structure function is derived, are plotted in Fig. 9 for the two ADCP instruments. The near-field zone boundary for these ADCPs, with transducer diameter of 61 mm and frequency of 1.2 MHz, would reach 74 cm, and thus regions up to this height above transducer were blanked. With the in-line mounting of the ADCPs adopted here, there is a possibility of interference from turbulence
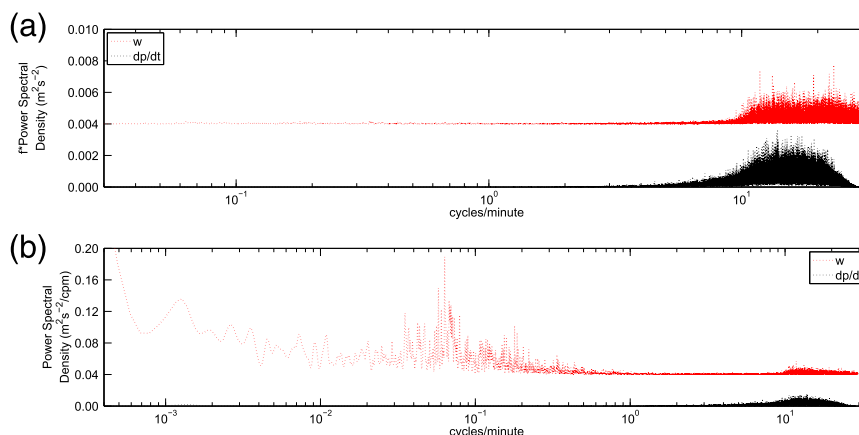

FIG. 8. Power spectral density of vertical velocity w from the upper ADCP ($\sim$22.5 m) and vertical motion of the buoy from the pressure sensor; w has an offset of 0.004 and 0.04, respectively, for plotting clarity: (a) in equal variance form, $[fP(f)$ versus $\log(f)]$, and (b) linear $P(f)$ versus $\log(f)$.
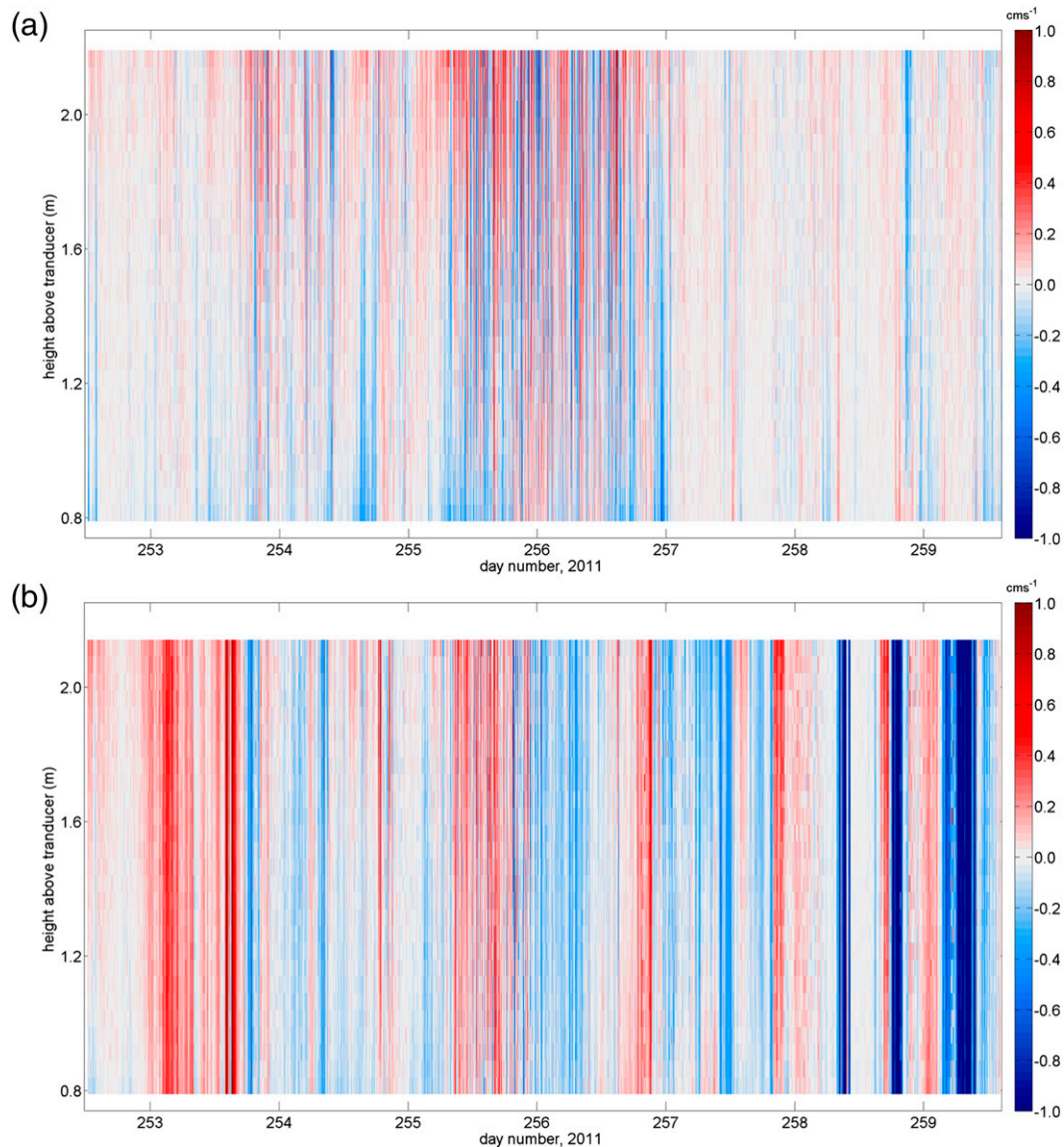
FIG. 9. The error velocities of the ADCP Earth coordinate output from which b' is derived: (a) the upper ADCP at $\sim$22.5 m and (b) the lower ADCP at $\sim$35.7 m. Both ADCP datasets are blanked from 0.74 to just above 2 m to remove the spurious data in the near and far field induced by phase variance and Microcat wake, respectively.

generated in the wake of instruments located higher up the mooring line. In the present case the upper and lower ADCPs were located $\sim$2.3 m below the base of the Microcat instruments, which have clearly generated spurious turbulence contributions in bins adjacent to these levels. Thus, the regions $\geq$2.19 m and $\geq$2.14 m for the upper and lower ADCP, respectively, were blanked to remove this interference signal.

The b' velocity data were used to calculate the structure function $D(z, r)$ [Eq. (1)] for each available bin by the application of a centered difference technique, squaring the velocities and then averaging over 5 min,

a time scale deemed long enough to provide an adequate sample while the turbulence can be assumed to remain statistically stationary. Examples of the structure function at different dissipation levels are shown in Fig. 10 together with the fitted $r^{2/3}$ curve. Since velocity estimates from adjacent bins are not independent, the structure function is computed at intervals of twice the bin separation ($\Delta r = \Delta z/\cos\theta = 10.6$ cm). In computing the fit, the range r is restricted to values less than 1 m, above which the data tend to deviate from the $r^{2/3}$ form, which according to theory is restricted to the inertial subrange. RDI standard deviation estimates obtained
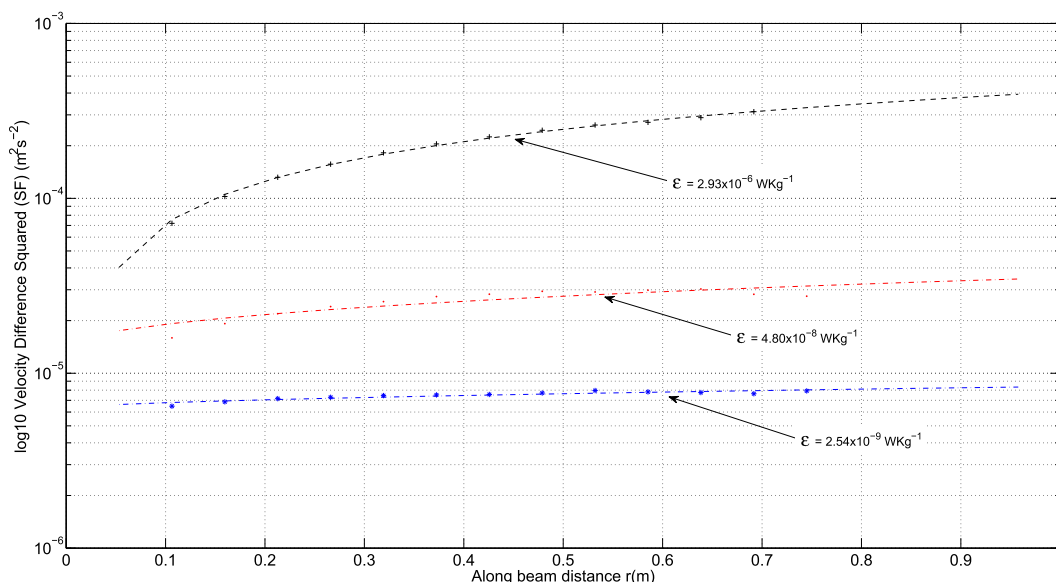
FIG. 10. Structure function data from 1-s ensembles of residual velocity data from the upper ADCP. The dotted lines are the fitted polynomials from Eq. (3) exhibiting an $r^{2/3}$ fit at three mean dissipation estimates: 2.93×10^{-6} W kg^{-1} (black), 4.80×10^{-8} W kg^{-1} (red), and 2.54×10^{-9} W kg^{-1} (blue).

from their proprietary software (Plan ADCP) gave figures of 0.43 cm s^{-1} for the upper ADCP and 0.77 cm s^{-1} for the lower ADCP, while the median noise level from the SF fit intercepts ($\equiv 2\sigma^2$) equates to 0.21 cm s^{-1} for the upper ADCP and 0.15 cm s^{-1} for the lower ADCP. Thus the Plan ADCP noise levels are 2 and 5 times higher for the upper and lower ADCPs, respectively.

The RDI software quotes the noise estimation based on separate pulse pairs. The SF noise estimations are obtained from samples separated along-beam, but using the same transmitted pulse pair and much of the same propagation path and thus are not completely independent. Consequently, the variance of the SF is somewhat reduced relative to the RDI figure. Turbulent kinetic energy (TKE) dissipation values derived from the structure function from each of the ADCP are presented in black in Fig. 11. In both plots, dissipation is seen to increase from low values ($\varepsilon \sim 10^{-9}$ W kg^{-1}) before the storm to maximum values ($\varepsilon \sim 10^{-5}$ W kg^{-1}) when the wind stress was at its peak on YD 255. A second maximum at the upper level (Fig. 11a) is apparent on YD 256 but is absent from the lower level. This difference reflects the fact that, whereas on YD 255 both instruments were in the same mixed layer, on YD 256 they were separated by a region of density stratification (see Fig. 4a), which seems to have inhibited the downward penetration of turbulence. After YD 256, the decline in wind stress led to diminishing levels of turbulence of similar magnitude to those at the start of the observation period.

d. Comparison with shear probe measurements

To compare dissipation derived from the structure function with values from the VMP shear probe, we have used vertically averaged values of ε from the SF and averages over the equivalent depth interval from the VMP profiles. The two independent estimates of ε, plotted together in Fig. 11, show a good degree of consistency over two decades of variation in dissipation in both the mean values and the variability of ε over short time scales. In comparing these estimates of dissipation, it is important to remember that the ADCP mooring and shipborne ADCP measurements were separated horizontally by a distance of ~ 1 km, as indicated in Fig. 2.

As an alternative comparison of the two ε measurements, we show the corresponding VMP and ADCP-SF values plotted against each other in Fig. 12. Here we have subtracted from the VMP measurements the instrument noise limit, quoted to be 3×10^{-10} W kg^{-1} (Rockland Scientific 2007). A neutral regression analysis (Garrett and Petrie 1981) of log10 ε gives a fit with a slope close to unity of 1.037 ± 0.01; mean ± 2 standard deviations (std) with considerable scatter (rms deviation ~ 0.50) from the regression line that reflects the short-term variability in both ε estimates (see Fig. 11).

6. Summary and discussion

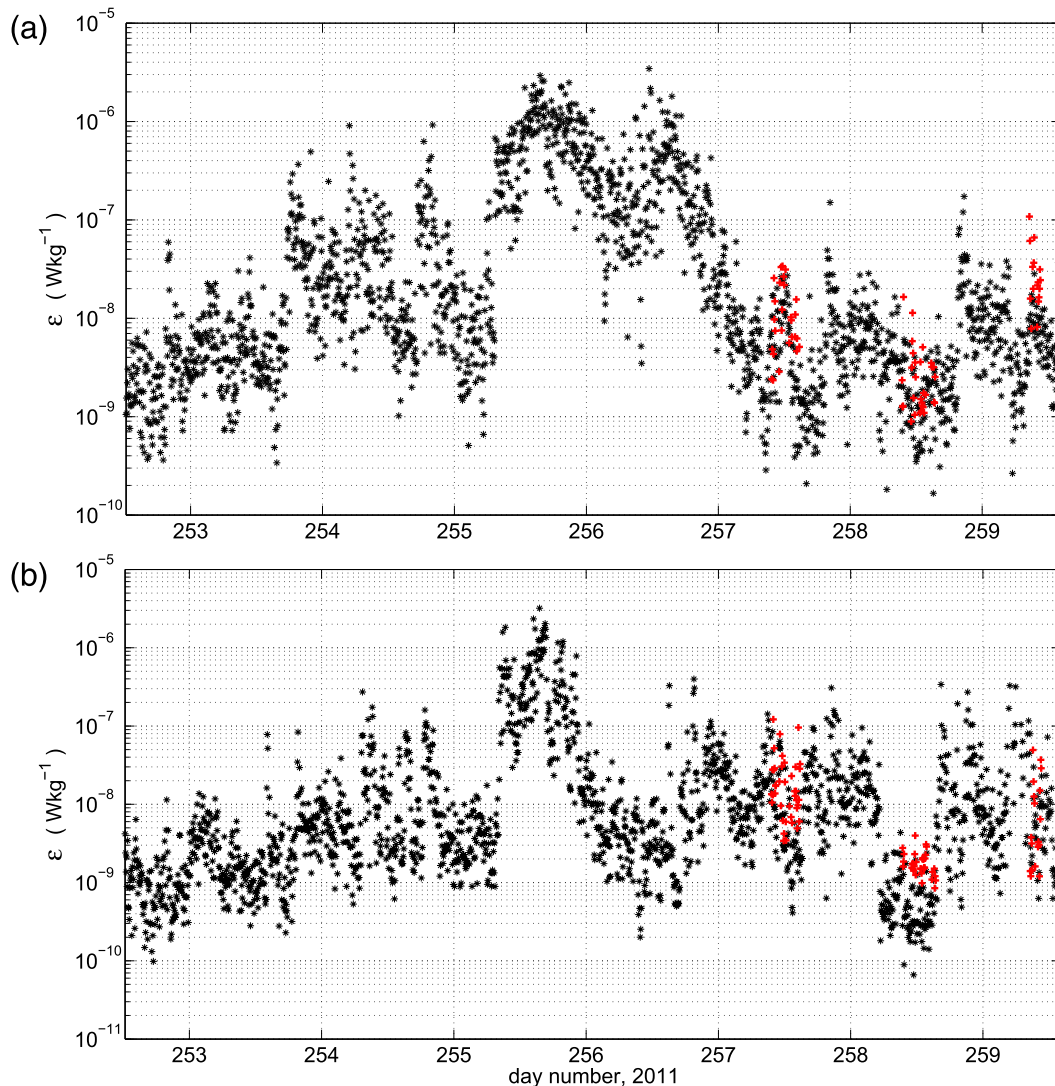The rate of dissipation of TKE ε has been determined by applying the structure function method to velocity

FIG. 11. Average energy dissipation ε (W kg^{-1}) from ADCP (black stars) and VMP ε (red crosses) (a) at the level of the upper ADCP, $\sim$22.5 m, and (b) at the level of the lower ADCP, $\sim$35.7 m.

data from pulse–pulse coherent ADCP instruments mounted in-line on a taut wire mooring for a period of 7 days. The resulting time series illustrates the variation of energy dissipation over $\sim$4 decades at two levels in the water column of the Clyde Sea before, during, and after the passage of a severe storm through the area. The validity of estimates of ε based on SF analysis of data from tethered ADCPs has been investigated by comparison with ε estimates from a VMP shear profiler operating nearby from a research vessel. Comparison of dissipation rates indicates generally good consistency between the two ε estimates over $\sim$2 decades. There is, however, considerable scatter, with similar variance in both datasets, which represents the inherent short-term variability of turbulence.

The noise floor of the SF method in our results does not appear to be significantly affected by motions of the mooring and is similar to that found in operation of ADCPs on fixed bed mountings (Mohrholz et al. 2008) and lower than the apparent noise characteristic of the VMP ($\sim$3 $\times$ 10^{-10} W kg^{-1}). Because it is based on difference measurements over small separations, we hypothesized that the SF method should not be degraded by the mooring motions. This hypothesis would seem to be confirmed by the good agreement of the dissipation estimates. For the same reason, the SF method minimizes contamination by the effects of surface waves (Trowbridge and Elgar 2003) because of the large vertical scale of such motions relative to the SF separation.
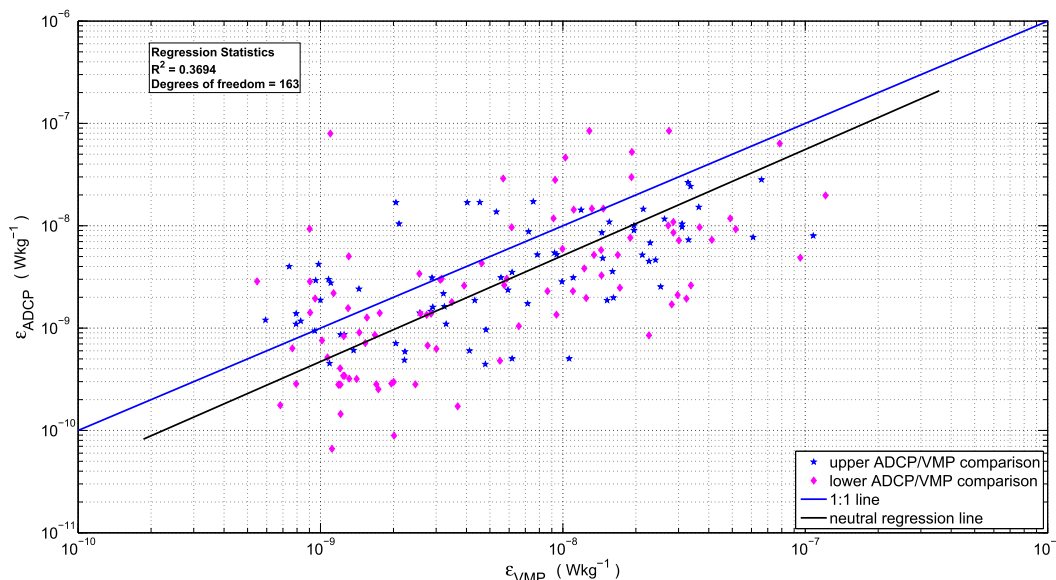
FIG. 12. TKE dissipation from ADCP structure function and VMP profiler for both upper and lower ADCPs. The 1:1 line (blue) and neutral regression line (black) (Garrett and Petrie 1981) are shown with statistical variables. The VMP values have the instrument noise level of $3 \times 10^{-10}\,\mathrm{W\,kg^{-1}}$ removed.

This comparison provides, for the first time, a clear illustration of the potential use of a pulse-to-pulse coherent ADCP instrument for the measurement of turbulent dissipation in the water column away from the bottom boundary. The technique is likely to be valuable for obtaining time series data in extreme weather conditions when, as in the storm documented here, operation of a shear profiler from a research vessel would not be possible. As originally implemented (Wiles et al. 2006), the structure function was based on data from each of the beams but where data have been recorded in Earth coordinates, as in the data used here, the error velocity may be used as representative turbulent velocity component in calculating the SF.

A possible concern in using the SF method is whether the results are influenced by the effects of stratification. Increased stratification will decrease the Ozmidov length L_o (see the introduction) and so with it the extent of the inertial subrange (ISR), which may then be smaller than the range over which the SF is calculated. To ensure the existence of an ISR, and with it, isotropy of the smaller eddies, the buoyancy Reynolds number $R_b = \varepsilon/(\nu N^2)$ should be greater than ~200, where ν is the kinematic viscosity of water (Gargett et al. 1984). In the observations reported here, this condition was satisfied when dissipation exceeded $10^{-9}\,\mathrm{W\,kg^{-1}}$ for much of the time except during periods of the lowest dissipation close to noise level ($\sim 10^{-10}\,\mathrm{W\,kg^{-1}}$) and the strongest stratification ($N^2 \sim 5 \times 10^{-4}\,s^{-2}$), when L_o was close to the bin size of $\Delta z = 0.05\,\mathrm{m}$. In principle, a lower

bin size can be selected to counter this problem but only at the expense of increased noise in the velocity measurements (Gargett and Moum 1995; Denman and Gargett 1983).

To achieve sufficiently low noise levels to determine dissipation in low energy flows, it is necessary to use pulse–pulse coherent modes of operation, which severely restrict the working range of the ADCP (in the present case to a few meters). In our study, we encountered a further limitation in range due to turbulence generated by other instruments attached to the mooring line above the ADCP. An ideal arrangement for avoiding this problem in future studies would be a mounting above the buoyancy at the top of the mooring string so that only uncontaminated turbulence is sampled.

REFERENCES

Baumert, H. Z., J. H. Simpson, and J. Sundermann, 2005: *Marine Turbulence: Theories, Observations, and Models.* Vol. 1, Cambridge University Press, 630 pp.

Burchard, H., O. Petersen, and T. P. Rippeth, 1998: Comparing the performance of the Mellor-Yamada and the k-ε two-equation turbulence models. *J. Geophys. Res.,* **103,** 10 543–10 554, doi:10.1029/98JC00261.

Denman, K. L., and A. E. Gargett, 1983: Time and space scales of vertical mixing and advection of phytoplankton in the upper

ocean. *Limnol. Oceanogr.,* **28,** 801–815, doi:10.4319/lo.1983.28.5.0801.

Gargett, A. E., and J. N. Moum, 1995: Mixing efficiencies in turbulent tidal fronts: Results from direct and indirect measurements of density flux. *J. Phys. Oceanogr.,* **25,** 2583–2608, doi:10.1175/1520-0485(1995)025<2583:MEITTF>2.0.CO;2.

——, T. R. Osborn, and P. W. Nasmyth, 1984: Local isotropy and the decay of turbulence in a stratified fluid. *J. Fluid Mech.,* **144,** 231–280, doi:10.1017/S0022112084001592.

Garrett, C. J. R., and B. Petrie, 1981: Dynamical aspects of the flow through the strait of Belle Isle. *J. Phys. Oceanogr.,* **11,** 376–393, doi:10.1175/1520-0485(1981)011<0376:DAOTFT>2.0.CO;2.

Gartner, J. W., and N. K. Ganju, 2002: A preliminary evaluation of near-transducer velocities collected with low-blank acoustic Doppler current profiler. *Proc. Conf. on Hydraulic Measurements and Experimental Methods,* Estes Park, Colorado, ASCE, doi:10.1061/40655(2002)17.

Gilcoto, M., E. Jones, and L. Fariña-Busto, 2009: Robust estimations of current velocities with four-beam broadband ADCPs. *J. Atmos. Oceanic Technol.,* **26,** 2642–2654, doi:10.1175/2009JTECHO674.1.

Howarth, M. J., and A. J. Souza, 2005: Reynolds stress observations in continental shelf seas. *Deep-Sea Res. II,* **52,** 1075–1086, doi:10.1016/j.dsr2.2005.01.003.

Inall, M. E., and T. P. Rippeth, 2002: Dissipation of tidal energy and associated mixing in a wide fjord. *Environ. Fluid Mech.,* **2,** 219–240, doi:10.1023/A:1019846829875.

Jackson, J. F. J., and A. J. Elliott, 2002: Internal waves in the Clyde Sea. *Estuarine Coastal Shelf Sci.,* **54,** 51–64, doi:10.1006/ecss.2001.0831.

Lacy, J. R., and C. R. Sherwood, 2004: Accuracy of a pulse-coherent acoustic Doppler profiler in a wave-dominated flow. *J. Atmos. Oceanic Technol.,* **21,** 1448–1461, doi:10.1175/1520-0426(2004)021<1448:AOAPAD>2.0.CO;2.

Lhermitte, R., and R. Serafin, 1984: Pulse-to-pulse coherent Doppler sonar signal processing techniques. *J. Atmos. Oceanic Technol.,* **1,** 293–308, doi:10.1175/1520-0426(1984)001<0293:PTPCDS>2.0.CO;2.

Li, W., C. Lancée, E. Cespedes, A. F. W. van der Steen, and N. Bom, 1997: Decorrelation of intravascular echo signals: Potentials for blood. *J. Acoust. Soc. Amer.,* **102,** 3785–3794, doi:10.1121/1.420141.

Lorke, A., 2007: Boundary mixing in the thermocline of a large lake. *J. Geophys. Res.,* **112,** C09019, doi:10.1029/2006JC004008.

——, L. Umlauf, and V. Mohrholz, 2008: Stratification and mixing on sloping boundaries. *Geophys. Res. Lett.,* **35,** L14610, doi:10.1029/2008GL034607.

Lu, Y., R. G. Lueck, and D. Huang, 2000: Turbulence characteristics in a tidal channel. *J. Phys. Oceanogr.,* **30,** 855–867, doi:10.1175/1520-0485(2000)030<0855:TCIATC>2.0.CO;2.

MacKinnon, J. A., and M. C. Gregg, 2003: Shear and baroclinic energy flux on the summer New England shelf. *J. Phys. Oceanogr.,* **33,** 1462–1475, doi:10.1175/1520-0485(2003)033<1462:SABEFO>2.0.CO;2.

Mohrholz, V., H. Prandke, and H. U. Lass, 2008: Estimation of TKE dissipation rates in dense bottom plumes using a Pulse Coherent Acoustic Doppler Profiler (PC-ADP)—Structure function approach. *J. Mar. Syst.,* **70,** 217–239, doi:10.1016/j.jmarsys.2007.03.004.

RD Instruments, 1998: ADCP coordinate transformation—Formulas and calculations. P/N 951-6079-00 (July), 26 pp.

Rippeth, T. P., E. Williams, and J. H. Simpson, 2002: Reynolds stress and turbulent energy production in a tidal channel. *J. Phys. Oceanogr.,* **32,** 1242–1251, doi:10.1175/1520-0485(2002)032<1242:RSATEP>2.0.CO;2.

——, J. H. Simpson, E. Williams, and M. E. Inall, 2003: Measurement of the rates of production and dissipation of turbulent kinetic energy in an energetic tidal flow: Red Wharf Bay revisited. *J. Phys. Oceanogr.,* **33,** 1889–1901, doi:10.1175/1520-0485(2003)033<1889:MOTROP>2.0.CO;2.

Rockland Scientific, 2007: VMP 500 Coastal Vertical Microstructure Profiler: Datasheet. Rockland Scientific, 2 pp. [Available online at http://rocklandscientific.com/VMP500/tabid/75/Default.aspx.]

Sauvageot, H., 1992: *Radar Meterology*. Artech House, 366 pp.

Sharples, J., M. C. Moore, T. P. Rippeth, P. M. Holligan, D. J. Hydes, N. R. Fisher, and J. H. Simpson, 2001: Phytoplankton distribution and survival in the thermocline. *Limnol. Oceanogr.,* **46,** 486–496, doi:10.4319/lo.2001.46.3.0486.

Simpson, J. H., and D. G. Bowers, 1984: The role of tidal stirring in controlling the seasonal heat cycle in shelf seas. *Ann. Geophys.,* **2** (4), 411–416.

——, W. R. Crawford, T. P. Rippeth, A. R. Campbell, and V. S. Cheok, 1996: The vertical structure of turbulent dissipation in shelf seas. *J. Phys. Oceanogr.,* **26,** 1579–1590, doi:10.1175/1520-0485(1996)026<1579:TVSOTD>2.0.CO;2.

——, P. J. Wiles, and B. J. Lincoln, 2011: Internal seiche modes and bottom boundary-layer dissipation in a temperate lake from acoustic measurements. *Limnol. Oceanogr.,* **56,** 1893–1906, doi:10.4319/lo.2011.56.5.1893.

Stacey, M. T., G. Monismith, and J. R. Burau, 1999: Measurements of Reynolds stress profiles in unstratified tidal flow. *J. Geophys. Res.,* **104,** 10 933–10 949, doi:10.1029/1998JC900095.

Trowbridge, J., and S. Elgar, 2003: Spatial scales of stress-carrying nearshore turbulence. *J. Phys. Oceanogr.,* **33,** 1122–1128, doi:10.1175/1520-0485(2003)033<1122:SSOSNT>2.0.CO;2.

Wiles, P. J., T. P. Rippeth, J. H. Simpson, and P. J. Hendricks, 2006: A novel technique for measuring the rate of turbulent dissipation in the marine environment. *Geophys. Res. Lett.,* **33,** L21608, doi:10.1029/2006GL027050.

Williams, E., and J. H. Simpson, 2004: Uncertainties in estimates of Reynolds stress and TKE production rate using the ADCP variance method. *J. Atmos. Oceanic Technol.,* **21,** 347–357, doi:10.1175/1520-0426(2004)021<0347:UIEORS>2.0.CO;2.

Zedel, L., A. E. Hay, R. Cabrera, and A. Lohrmann, 1996: Performance of a single-beam pulse-to-pulse coherent Doppler profiler. *IEEE J. Oceanic Eng.,* **21,** 290–297, doi:10.1109/48.508159.